Journal of Multidisciplinary Engineering Science and Technology (JMEST)
ISSN: 2458-9403
Vol. 10 Issue 4, April - 2023

KYAMOS Software – Compressible Finite Volume, Total Variation Diminishing Solver

[1,2]Antonis P. Papadakis, [1]Aimilios Ioannou, [1]Sofia Nikolaidou, and [1,2]Wasif Almady
[1]KYAMOS LTD, 37 Polyneikis Street, Strovolos, 2047, Nicosia, Cyprus
[2]Frederick University, 7. Y. Frederickou Steet, 1036, Palouriotissa, Nicosia, Cyprus

***Abstract*— In this paper, an innovative Euler-based equation solver is developed based on the finite volume, total variation, diminishing method (FV-TVD). It is a combination of Van-Leer and HLL limiters, combined with the second order Runge-Kutta Heun's method. The new solver can capture compressible shock waves accurately. Validation of the algorithm and the implemented software is performed using the well-known Sod shock tube test case, one of the few methods that there is an analytical solution, demonstrating the ability of the algorithm to capture the shocks of density, velocity, energy, and pressure. Direct comparisons between simulated and theoretical shock tube results are calculated.**

Keywords—Finite Volume; Total Variation Diminishing; compressible flows; shock waves; Sod shock tube;

I. INTRODUCTION

KYAMOS objective is to develop disruptive engineering multiphysics software for scientists, academics, researchers, engineers, and non-engineers to develop and optimize engineering systems and devices within the Computer Aided Engineering (CAE) industry. To establish KYAMOS LIMITED as a competitive, innovative multiphysics software company at an international level for computational excellence in speed and accuracy, it needs to offer disruptive technologies that will outperform its competitors. We have recently built a state-of-the-art finite volume method that solves the convection-diffusion equation using an innovative combination of Superbee and Van Leer limiters for compressible flows based on the Total Variation Diminishing (TVD) scheme. The TVD scheme can capture Gaussian and cubic waves motion ideally, after 10,000 time steps in linear wave propagation [1]. In this paper, we wish to develop it into a fully compressible Euler based solver that can solve non-linear phenomena, accurately. Hence, in this paper, a proprietary multiphysics solution using the Finite Volume, TVD (FV-TVD) method has been developed to provide meaningful simulations regarding highly compressible flows.

Specifically, the mathematical formulation for solving FV-TVD equations in compressible flows is first developed and translated to computer simulation software. To test whether the software works in simulating compressible flow propagation, we have tested the software using the well-known benchmark compressible flow test case of the Sod shock tube. The

Sod shock tube test case is one of the few compressible problems in computational fluid dynamics where there is an analytical solution.

The different elements of the method have been tested such as the core code, the treatment of initial and boundary conditions, and its ability to capture compressible flows.

The main drive behind this work is that FV-TVD solvers have recently gained increased attention and many papers are published regarding the capabilities of this method and even used from our competitors (open source OPENFOAM and proprietary ANSYS), when compared to the traditional Finite Difference, Finite Element and Finite Volume methods. We wish to test this technology on cloud-based distributed GPU computing that will unleash its real capabilities through CUDA aware MPI and deep learning techniques and apply it in practical simulations such as the compressible behavior of automotives, rockets, airplanes, etc.

II. FINITE VOLUME

The macroscopic simulation world encompasses the solution of three types of partial differential equations: (a) parabolic, (b) elliptic, and (c) hyperbolic. There are mainly three widely known methods for the solution of the above equations which are the finite difference, finite element, and finite volume methods, each one with its advantages and disadvantages. Generally, at KYAMOS, we utilize state-of-the-art method from a commercialization perspective, i.e., the finite element method which is the most accurate method for the simulation of elliptic field problems and the finite volume, the prevailed method for the simulation of fluid flow problems due to its conservative nature. Finite difference is considered as an inferior alternative to the above methods, well-known nevertheless for its simplicity, but nevertheless, non-state-of-the-art, in most of the simulation cases.

The FV methods provide an attractive alternative which is generally applicable to transient flows due to their conservative nature, which makes them ideal for fluid flow simulations. They are based on a continuum assumption of the macroscopic fluid properties and can be partitioned easily, without the need for the solution of matrices which are ill-conditioned (depends on scheme) and it is ideal for parallelization, especially on the GPUs.

Regarding fluid flow simulations, a new innovative state-of-the-art approach for capturing shocks is the Godunov type method that encompasses the Total Variation Diminishing (TVD) scheme. We have recently developed such a scheme that could potentially outstrip our competitors, which either use non-efficient shock capturing schemes in the finite element or finite volume basis.

We would like to utilize this state of the art, FV-TVD scheme which is able to capture in a conservative way shock waves with no oscillations and numerical diffusion and utilize it in compressible flow simulations. We can capture both the propagation of the shock, as well as the rarefraction wave in near ideal conditions, since after many time steps, there is considerable agreement between analytical and simulated results. We also believe that we can further improve our algorithm to achieve much better overall agreement between analytical and numerical results by deploying an innovative interpolation scheme between the above two limiters.

We expect that the highly accurate compressible flow software to be developed will be competitive against our industrial competitors and will outstrip them by utilizing a newly developed promising technique, an alternative to other techniques out there.

We do not expect that we can compete with multimillion-dollar companies in terms of software modules and variety of solutions, at least in the beginning; however, we believe that we can give a formidable alterative to a few specific areas such as compressible flow simulations, until KYAMOS has the resources to expand at the next level, by offering broader simulation solutions for a number of industries.

III. LIRERATURE REVIEW ON THE FV-TVD

Various projects were conducted to better understand the effect of flux limiters on reduced total variation (TVD) schemes under different circumstances. In this paper [2], the authors explore a kind of higher-order Runge-Kutta time discretization with reduced total variation (TVD) initialized in Shu & Osher (1988), which is suitable for solving conservation laws with stable spatial discretizations. The authors illustrate through numerical examples that a non-TVD, but linearly stable Runge-Kutta time discretization scheme, can produce oscillations, even for a TVD spatial discretization. This verifies the fact that TVD Runge-Kutta methods are necessary to minimize oscillations. The authors then explore the effects of second, third and fourth orders and low-storage Runge-Kutta methods.

In addition, a study conducted in 2019 [3], investigates the total variation diminishing (TVD) scheme for multi-species transport with first-order reaction network in multi-dimensional space. The partial differential equations describing this multispecies transport with chain reactions in the form of a coupled system are presented. The system is then solved by a TVD scheme with different limiters. Finally, the necessary criteria for the scheme to be TVD qualified are derived.

In 2022, S. A. Alimuddin et al. suggest that the choice of limiters has a significant impact on the behavior of the Davis-Yee and Harten-Yee TVD schemes [4]. The authors performed a series of simulations using various test cases, including the 1D advection equation, the shock tube problem, and the two-dimensional lid-driven cavity flow. The study concludes that the minmod limiter produces the most accurate and stable results for both the Davis-Yee and Harten-Yee schemes and reduces the spurious oscillations that can occur when using TVD schemes. On the other hand, the superbee limiter tends to produce inaccurate and unstable solutions, with oscillations in regions with steep gradients. Lastly, the van Leer limiter is found to be less accurate and less stable than the minmod limiter, but more accurate and stable than the superbee limiter.

Another study was conducted in 2022, S. Kaewta et al. focused on “a comparison of TVD limiter functions for a convection–diffusion–reaction equation and Euler equations on triangular grids” [5]. To test the accuracy and stability of the limiters, several pure convection and convection–diffusion–reaction problems were solved on both structured and unstructured triangular grids. From this study, it was found that the limiters applied to solve Euler equations yield great results for both linear and nonlinear problems. During the same year, L. Bessone et al. [6] successfully implemented Eulerian TVD methods and applied parallelization strategies based entirely on GPU to generate exponentially correlated log-normally distributed permeability fields in C++/CUDA. The authors consider pure advection, advection-diffusion, and advection-dispersion. The results of this study suggest that the algorithms can efficiently work in computational domains of up to 134.5 million cells in a single GPU.

Additionally, in 2021, L. Krivodonova and A. Smirnov focused “on the TVD property of second-order methods for 2D scalar conservation laws” [7]. In this paper, the authors utilized the second-order discontinuous Galerkin method to numerically prove that limited solutions of two-dimensional hyperbolic equations are TVD in means when total variation is computed using a definition arising from a full discretization of the semi-discrete Raviart-Thomas TV.

In another study of 2019, Ali et al. investigated “Finite Volume TVD Scheme for a Nonlinear Gas Transport Model in Shale Rocks” [8]. The authors developed a conservative finite volume TVD scheme to obtain the numerical solutions of the gas transport model. In order to determine the numerical solutions to a nonlinear gas transport model, the numerical model is applied to a time-dependent advection-diffusion equation.

Recent research on the “Comparison of Errors Caused by Flux Limiters on the Numerical Solution of Advection-Diffusion Problem” was conducted by A. Tasri [9]. This article proposes a method for applying one-dimensional limiters to two-dimensional unstructured mesh and discusses the errors caused by various flux limiters in advection-diffusion flow solutions. The results suggest that there was a higher

calculation error of second-order finite volume with a flux limiter than the one without a limiter. On the other hand, the error of second-order finite volume without a flux limiter was higher than the error of third-order with a flux limiter. Summing up, in this article, Venkatakrishnan's flux limiter was found to produce the highest error, followed by Van Leer's limiter, EULER and SMART limiter.

There are also many projects that went beyond TVD and proposed different or more complex flux schemes. A research paper, titled "Capturing of Shock Wave of Supersonic Flow over the Bump Channel with TVD, ACM and Jameson Methods", written by M. Yadegari and M.H. Jahdi in 2021 [10] introduced a method based on the characteristic variables (Riemann solution) and controlled the diffusion term in the classic methods to capture the shock waves. The authors used a non-orthogonal mesh with collocated finite volume formulation, a method based on the density-based algorithm, to solve the compressible Euler equations. The study corroborates that the ACM and TVD methods achieved a higher resolution of the shock waves than the Jameson method. Additionally, these two methods improved the quality of shock waves capturing all flows at the discontinuities, and the computational time and convergence of the supersonic flows.

In 2019, R. Lochab and V. Kumar presented a numerical formulation of shallow water equations (SWEs) using a fuzzy logic-based flux limiting scheme [11]. The dam-break problem with flat bottom topography was implemented to test the effectiveness and accuracy of the proposed scheme. The authors suggest that the proposed high-resolution (HR) method is non-oscillatory, conservative, and suitable for shallow water models. The results presented good agreement with analytical solutions and the proposed scheme was able to capture both smooth and discontinuous profiles, leading to better oscillation-free results.

Furthermore, S. Tang and M. Li authored a paper of "Construction and application of several new symmetrical flux limiters for hyperbolic conservation law", focusing on combining the classical van Albada, van Leer, and PR-κ limiters with the MAX function to create three symmetrical limiter functions [12]. The constructed limiters were found to produce more accurate results than classical limiters. It is suggested that the Monotonic Upstream-centered Scheme for Conservation Laws (MUSCL scheme) along with the proposed limiters satisfies the conditions for quadratic convergence in smooth regions. The MUSCL scheme equipped with classic limiters corresponding to both smooth and discontinuous solutions was found to exhibit lower resolution and higher dissipation than the scheme equipped with the new symmetrical limiters.

A recent study by I. F. Ismail et al. [13] focuses on developing first-order Flux Vector Splitting (FVS) schemes and extending the solution capabilities to flow with two shocks, like the Woodward-Collela blast wave problem. The execution of three FVS schemes, Steger-Warming, Van Leer, and Liou-Steffen, resulted in different flow patterns with respect to each test case's extremities. The Steger-Warming scheme was found to produce the largest dissipation over one-dimensional test cases. The most accurate for capturing shocks, with very few overshoots and undershoots, was the Liou-Steffen scheme. The outcomes of this scheme showed oblique shock waves at the compression corners and expansion waves at the expansion corners. Lastly, the results implied that bow shocks can be simulated using the blunt-body geometry and one- and two-dimensional results confirm the shock-capturing ability of these schemes.

Lastly, Osman ÜNAL modified TCDF to propose a novel flux limiter in 2022, as presented in the paper "Numerical Simulation of Convection-Diffusion Equation Using a Novel Flux Limiter" [14]. The results of this study showed that the modified TCDF flux limiter function worked at a Courant number lower than one without any abnormal oscillation, in contrast to the previously improved TCDF flux limiter. This study also aimed to present a numerical simulator for solution of convection-diffusion equation, for any grid dimension or any space or time interval.

IV. Navier–Stokes and Euler equations

The Euler equations are special partial differential equations set of Navier–Stokes equations (NS), where the viscosity and conductivity terms are zero. They can be used for compressible and incompressible flows. By considering the conservation form of the Navier–Stokes continuity equation:

$$\frac{\partial \rho}{\partial t} + \nabla.(\rho u) = 0 \tag{1}$$

For two-dimensions, eq (1) can be expanded as follows:

$$\frac{\partial \rho}{\partial t} + \frac{\partial \rho u_x}{\partial x} + \frac{\partial \rho u_y}{\partial y} = 0 \tag{2}$$

, where ρ represents the density, u is the velocity, u_x and u_y are the components of the velocity vector.

The continuity equation will be the same for the Euler equation, since there are no viscosity and conductivity terms. Considering the conservation form of the Navier–Stock momentum equation for compressible flows:

$$\frac{\partial \rho u}{\partial t} + \nabla \cdot (\rho u \otimes u) = -\nabla P + \frac{1}{3}\mu \nabla(\nabla.u) + \mu \nabla^2 u + \rho g \tag{3}$$

where μ represents the kinematic viscosity, P is the pressure which represents the internal sources, and g is a vector that represents the body acceleration multiplied by the density, and the product represents the external force. If we set the viscosity term to zero, eq (3) becomes:

$$\frac{\partial \rho u}{\partial t} + \nabla \cdot (\rho u \otimes u) + \nabla P = \rho g \quad (4)$$

For two-dimensions, eq (4) can be expanded:

$$\begin{pmatrix} \frac{\partial \rho u_x}{\partial t} \\ \frac{\partial \rho u_y}{\partial t} \end{pmatrix} + \begin{pmatrix} \frac{\partial}{\partial x} \\ \frac{\partial}{\partial y} \end{pmatrix} \cdot \left(\rho \begin{pmatrix} u_x \\ u_y \end{pmatrix} \begin{pmatrix} u_x & u_y \end{pmatrix} \right) + \begin{pmatrix} \frac{\partial P}{\partial x} \\ \frac{\partial P}{\partial y} \end{pmatrix} = \rho \begin{pmatrix} g_x \\ g_y \end{pmatrix} \rightarrow \quad (5)$$

$$\begin{pmatrix} \frac{\partial \rho u_x}{\partial t} \\ \frac{\partial \rho u_y}{\partial t} \end{pmatrix} + \begin{pmatrix} \frac{\partial}{\partial x} \\ \frac{\partial}{\partial y} \end{pmatrix} \cdot \left(\rho \begin{pmatrix} u_x \\ u_y \end{pmatrix} \begin{pmatrix} u_x & u_y \end{pmatrix} \right) + \begin{pmatrix} \frac{\partial P}{\partial x} \\ \frac{\partial P}{\partial y} \end{pmatrix} = \rho \begin{pmatrix} g_x \\ g_y \end{pmatrix} \rightarrow \quad (6)$$

$$\begin{pmatrix} \frac{\partial \rho u_x}{\partial t} \\ \frac{\partial \rho u_y}{\partial t} \end{pmatrix} + \begin{pmatrix} \frac{\partial}{\partial x} \\ \frac{\partial}{\partial y} \end{pmatrix} \cdot \left(\rho \begin{pmatrix} u_x u_x & u_x u_y \\ u_x u_y & u_y u_y \end{pmatrix} \right) + \begin{pmatrix} \frac{\partial P}{\partial x} \\ \frac{\partial P}{\partial y} \end{pmatrix} = \rho \begin{pmatrix} g_x \\ g_y \end{pmatrix} \rightarrow \quad (7)$$

$$\begin{pmatrix} \frac{\partial \rho u_x}{\partial t} \\ \frac{\partial \rho u_y}{\partial t} \end{pmatrix} + \begin{pmatrix} \frac{\partial \rho u_x u_x}{\partial x} + \frac{\partial \rho u_x u_y}{\partial y} \\ \frac{\partial \rho u_x u_y}{\partial x} + \frac{\partial \rho u_y u_y}{\partial y} \end{pmatrix} + \begin{pmatrix} \frac{\partial P}{\partial x} \\ \frac{\partial P}{\partial y} \end{pmatrix} = \rho \begin{pmatrix} g_x \\ g_y \end{pmatrix} \rightarrow \quad (8)$$

$$\begin{pmatrix} \frac{\partial \rho u_x}{\partial t} \\ \frac{\partial \rho u_y}{\partial t} \end{pmatrix} + \begin{pmatrix} \frac{\partial \rho {u_x}^2}{\partial x} + \frac{\partial \rho u_x u_y}{\partial y} \\ \frac{\partial \rho u_x u_y}{\partial x} + \frac{\partial \rho {u_y}^2}{\partial y} \end{pmatrix} + \begin{pmatrix} \frac{\partial P}{\partial x} \\ \frac{\partial P}{\partial y} \end{pmatrix} = \rho \begin{pmatrix} g_x \\ g_y \end{pmatrix} \quad (9)$$

, where g_x and g_y are the components of the gravity vector.

Eq (9) is the conservation form of the Euler momentum equation.

The energy equation of the Euler equation without the force term becomes:

$$\frac{\partial E}{\partial t} + \nabla \cdot \big((E+P)u\big) = 0 \quad (40)$$

$$\frac{\partial E}{\partial t} + \begin{pmatrix} \frac{\partial}{\partial x} \\ \frac{\partial}{\partial y} \end{pmatrix} \cdot \left((E+P) \begin{pmatrix} u_x \\ u_y \end{pmatrix} \right) = 0 \quad (51)$$

$$\frac{\partial E}{\partial t} + \frac{\partial (E+P)u_x}{\partial x} + \frac{\partial (E+P)u_y}{\partial y} = 0 \quad (62)$$

Generally, the Euler equations in two-dimensions compressible flows can be written as:

$$\frac{\partial U}{\partial t} + \frac{\partial F_x}{\partial x} + \frac{\partial F_y}{\partial y} = K \quad (73)$$

, where U represents the conservative variables:

$$U = \begin{pmatrix} \rho \\ \rho u_x \\ \rho u_y \\ E \end{pmatrix} \quad (84)$$

F_x and F_y represent the flux variables:

$$F_x = \begin{pmatrix} \rho u_x \\ \rho {u_x}^2 + p \\ \rho u_x u_y \\ (E+P)u_x \end{pmatrix}, F_y = \begin{pmatrix} \rho u_y \\ \rho u_x u_y \\ \rho {u_y}^2 + p \\ (E+P)u_y \end{pmatrix} \quad (95)$$

The source term K becomes:

$$K = \begin{pmatrix} 0 \\ \rho g_x \\ \rho g_y \\ 0 \end{pmatrix} \quad (106)$$

If we neglect the gravitational force, there are five primitive variables and four conservation equations. In order to close the system of equations, we need an additional equation, which is the equation of state:

$$E = \frac{P}{\gamma - 1} + \frac{\rho u^2}{2} \quad (117)$$

, where γ represents the ratio of specific heats, which in this paper is taken as 1.4, the specific heat of air.

V. Mathematical Formulation of Finite Volume Method (FVM)

The starting point of the finite volume method is the integral form of the conservation form of partial differential equations. Therefore, the Euler equations can be rewritten by neglecting the term of the gravitational force in integral form as follows:

$$\frac{\partial U}{\partial t} + \frac{\partial F_x}{\partial x} + \frac{\partial F_y}{\partial y} = 0 \rightarrow \quad (128)$$

$$\frac{\partial U}{\partial t} + \nabla \cdot F = 0 \rightarrow \quad (139)$$

$$\int \frac{\partial U}{\partial t} dV + \int \nabla \cdot F dV = 0 \quad (20)$$

, where V represents the volume of the cell. The integration in the finite volume method is based on the control volume of the unit cell, so the domain will be discretized into discrete control volumes. Each control volume will have a centroid, which represents the values of the primitive variables, and boundary, which represents the values of the fluxes. The cell center is commonly indexed as i, while the faces are indexed as i+1/2 and i-1/2. Now we can integrate over the control volume, with eq (20) becoming:

$$\int_{i-\frac{1}{2}}^{i+\frac{1}{2}} \frac{\partial U_i}{\partial t} dV_i + \int_{i-\frac{1}{2}}^{i+1} \nabla \cdot F \, dV_i = 0 \quad (21)$$

For the time derivative, the average value of the primitive variables is assumed to be calculated at the

center of control volume, and by using the mean value theory:

$$\bar{U}_i = \frac{1}{V_i}\int_{V_i} U_i dV_i \rightarrow \quad (22)$$

By inserting the time derivative on both sides of eq (22), eq (22) becomes:

$$\frac{\partial}{\partial t}\bar{U}_i = \frac{\partial}{\partial t}\frac{1}{V_i}\int_{V_i} U_i dV_i \rightarrow \quad (23)$$

$$\frac{\partial \bar{U}_i}{\partial t} = \frac{1}{V_i}\int_{V_i} \frac{\partial U_i}{\partial t} dV_i \quad (24)$$

By using the divergence theory, the term of the flux can be converted into integral surfaces:

$$\int_{i-\frac{1}{2}}^{i+\frac{1}{2}} \nabla \cdot F \, dV_i = \oint_{S_i} F.n \, dS \quad (25)$$

, where S in a three-dimensional illustration represents the total surface area, in a two-dimensional illustration represents the length of the edges, and n is the unit vector normal to the surface pointing outward of the surface. The mean value theorem can be used to approximate the surface integral, with eq (25) becoming:

$$\oint_i F.n \, dS = \sum_{f_1,f_2....} \bar{F}_f \cdot n_f \, dS_f \quad (26)$$

, where f represents the faces of the two-dimensional control volume, and $\bar{F}_f$ is the average value of the flux. The number of the faces will depend on the type of the mesh that will be used. Combining the above equations, we get:

$$\frac{\partial \bar{U}_i}{\partial t} V_i + \sum_{f_1,f_2....} \bar{F}_f \cdot n_f \, dS_f = 0 \quad (27)$$

$$\frac{\partial \bar{U}_i}{\partial t} = -\frac{1}{V_i}\sum_{f_1,f_2....} \bar{F}_f \cdot n_f \, dS_f \quad (28)$$

Eq (28) can be approximated using the second order Runge-Kutta Heun's method. The value of the slope (gradient) is used at the initial value of the conservative values and t_o=0 to extrapolate the values of the conservative values at one time step. Then, the resultant values are required to evaluate the slope at one time step, by averaging the values of the slope. The estimation of the new values can be defined as follows:

$$K_1 = -\frac{1}{V_i}\sum_{f_1,f_2....} \bar{F}_f{}^{t_0} \cdot n_f \, dS_f \quad (29)$$

$$K_2 = -\frac{1}{V_i}\sum_{f_1,f_2....} \bar{F}_f{}^{t_1}\left(\bar{U}_i^{t_0} + hK_1\right) \cdot n_f \, dS_f \quad (30)$$

$$\bar{U}_i^{t_1} = \bar{U}_i^{t_0} + h\frac{(K_1 + K_2)}{2} \rightarrow \quad (31)$$

$$\bar{U}_i^{t_{n+1}} = \bar{U}_i^{t_n} + h\frac{(K_1 + K_2)}{2} \quad (32)$$

, where K_1 represents the slop at t_o, K_2 represents the slope at one time step, $\bar{F}_f{}^{t_0}$ represents the flux at t_o, non-negative integers, $\bar{F}_f{}^{t_1}\left(\bar{U}_i^{t_0} + hK_1\right)$ represents the flux at one time step and $\bar{U}_i^{t_0} + hK_1$, and h represents the time step equal to Δt.

VI. Results of FV-TVD Simuations

A. Introduction

In this section, simulated results using the innovative FV-TVD method are compared to analytical solutions regarding the Sod shock tube problem. Error calculations are also included which show the accuracy of the proposed method in capturing the shocks.

In the Sod shock tube test case, we observe five distinct regions, as a result of the propagation of a shock wave in a compressible gas flow problem. The five distinct regions are:

1. Undisturbed left ambient region: It is defined as the initial high-pressure region of the compressible gas that is not affected by the shock wave or expansion fan wave.
2. Shocked left region: It is defined as the region which resides between the shock wave and the contact discontinuity, where the gas is compressed by the advancing shock wave.
3. Contact discontinuity: The contact discontinuity is defined as a thin region which separates the shocked left and right gas sides. In the case of pressure and of velocity, the profile is continuous, whereas the density usually exhibits discontinuous behavior.
4. Shocked right region: This is the region between the contact discontinuity and the head of the expansion fan, where the gas has been accelerated and rarefied by the expansion fan.
5. Undisturbed right ambient region: It is defined as the initial high-pressure region on the right of the compressible gas that is not affected by the shock wave or expansion fan wave.

B. Results and discussion

Fig. 1 presents the fluid pressure propagation through the Sod shock tube at time 0.2 s in two-dimensions. The graph shows that the results are invariant in the y-direction, as expected, with the pressure remaining unchanged. This also shows that the boundary conditions being implemented were of the correct nature. The boundary conditions used for the simulation of the Sod shock tube were the Neumann boundary conditions on the top and bottom surfaces. Similar boundary conditions were also implemented at the left and right boundary of the tube, since the simulations were stopped prior to the shock and rarefraction wave heating the boundary. In such a case, one will need to deploy appropriate boundary conditions, i.e., for example if indeed is a closed tube,

no-slip boundary conditions should be applied at the left, right, top and bottom boundaries and this would affect the propagation of the shock from the beginning of the simulation, since a layer of low velocity would occur on the top and bottom surfaces during the rarefraction and shock wave propagation.

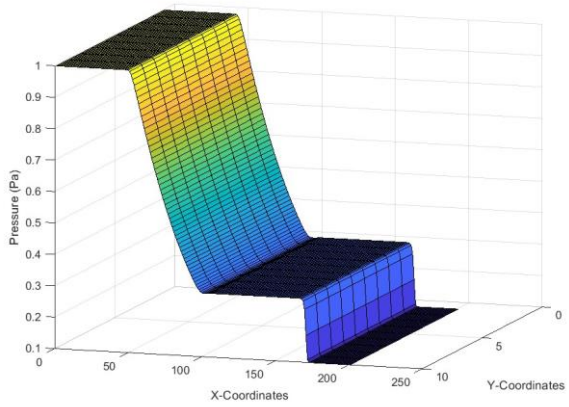

Fig. 1 Simulated fluid pressure propagation through the Sod shock tube at time 0.2 s.

Fig. 2 presents the simulated fluid density propagation through the Sod shock tube at time 0.2 s. Similarly to the pressure, the fluid density in the y-direction exhibits uniformity, as expected. Additionally, the density in contrast to the pressure exhibits an additional plateau, as a result of the contact discontinuity, which creates an extra region, separating the left and right shock wave regions.

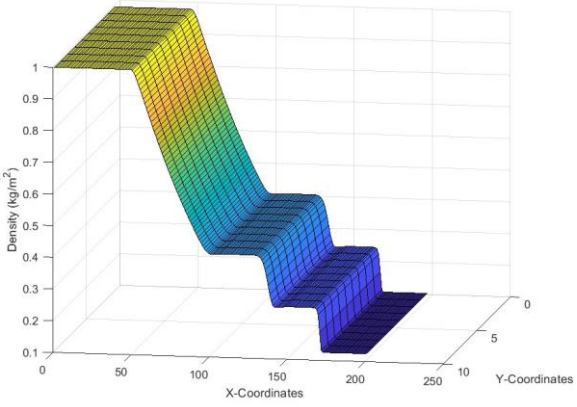

Fig. 2 Simulated fluid density propagation through the Sod shock tube at 0.2s.

Fig. 3 shows the velocity propagation through the Sod shock tube at time 0.2 s. The velocity shows a similar profile with the pressure where there is no change across the contact discontinuity. The velocity values of the wave are all positive as expected and are less abrupt at the boundary between the undisturbed left region with the shocked left region, when compared to the boundary between the shocked right region and the undistracted right region. Again, the velocity does not show variation in the y-direction as expected, similarly to the density and the pressure profiles.

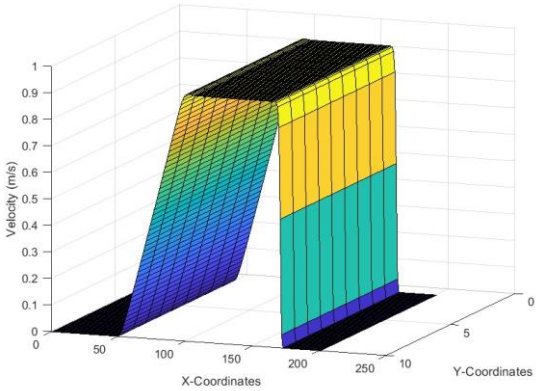

Fig. 3 Simulated fluid velocity propagation through the Sod shock tube at 0.2s.

To conclude, the FV-TVD algorithm in its two-dimensional representation seems to accurately predict the fluid flow in a Sod shock tube after comparing the results with expected values.
Fig. 4 shows the simulated fluid pressure propagation profile through the Sod shock tube (red line) compared with the exact solution (blue) at 0.2 s. Fig. 4 shows that there is a close relationship between the analytical and numerical results, validating the performance of our FV-TVD code. The results, as expected, struggle slightly to capture the discontinuities in general.

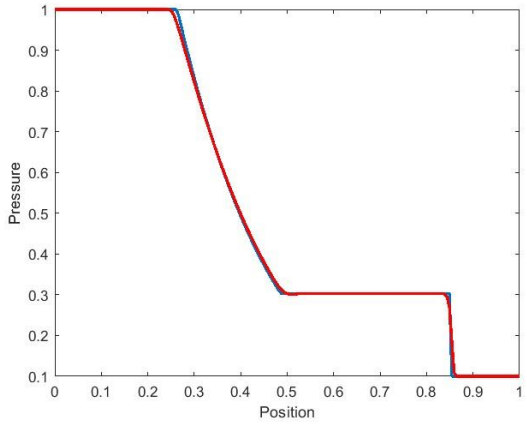

Fig.4 Simulated fluid pressure propagation profile through the Sod shock tube (red) compared with the exact solution (blue) at 0.2 s.

Fig. 5 shows the simulated fluid density propagation profile through the Sod shock tube (red line) compared with the exact solution (blue) at 0.2 s. Fig. 5 shows that there is a close relationship between the analytical and numerical results, validating the performance of our FV-TVD code. The results, as expected, struggle slightly to capture the discontinuity in general. The largest error occurs at the discontinuity boundary, as expected.

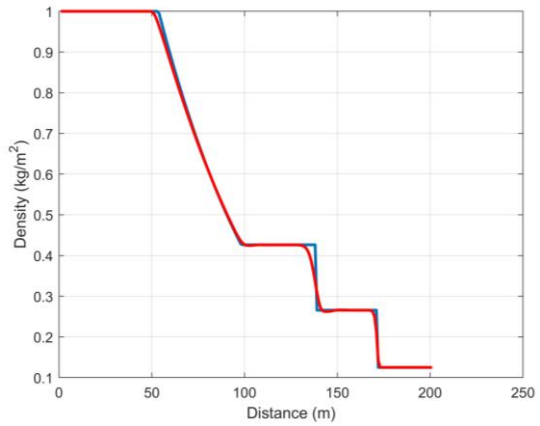

Fig. 5 Simulated fluid density propagation profile through the Sod shock tube (red) compared with the exact solution (blue) at 0.2s.

Fig. 6 shows the simulated fluid velocity propagation profile through the Sod shock tube (red line) compared with the exact solution (blue) at 0.2 s. Fig. 6 shows that there is a close relationship between the analytical and numerical results. There is a slight difference in the region between the undisturbed left region and the left shock ware region boundary. The results, in the other two discontinuity boundary exhibit more accurate results.

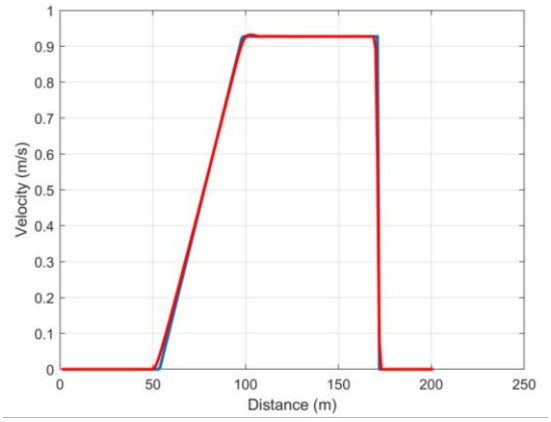

Fig. 6 Simulated fluid velocity propagation profile through the Sod shock tube (red) compared with the exact solution (blue) at 0.2s.

VII. Conclusions

In this paper, we demonstrate the implementation of an innovative FV-TVD scheme by validating it against the analytical solution in the Sod shock tube test case. The results evidently show very good agreement with the analytical solution and demonstrate the potential of the solver to be used for commercial purposes by embedding the solver in the KYAMOS software. Further work should include the extension of the solver in thee-dimensions, as well as the deployment in a distributed environment, and most importantly to be included within the Graphical User Interface (GUI) of KYAMOS software as a module for simulating compressible fluid flows.

Acknowledgment

This work was co-funded by the European Regional Development Fund of the European Union and the Republic of Cyprus through the Research and Innovation Foundation (Project: REALISATION-COMPRESSIBLE-GPU-AI CONCEPT/0521/0045).

References

[1] A. P. Papadakis, A. Ioannou, and W. Almady, "KYAMOS Software - Finite Volume TVD scheme for advection fluid simulations," *Journal of Multidisciplinary Engineering Science and Technology*, vol. 7, no. 12, pp. 13222-13232, 2020.

[2] S. Gottlieb and C.-W. Shu, "Total variation diminishing Runge-Kutta schemes," *Mathematics of computation*, vol. 67, no. 221, pp. 73-85, 1998.

[3] S. Prabhakaran and L. Jones Tarcius Doss, "Total Variation Diminishing Finite Volume Scheme for Multi Dimensional Multi Species Transport with First Order Reaction Network," in *Mathematical Analysis and Computing: ICMAC 2019, Kalavakkam, India, December 23–24*, 2021, pp. 481-498: Springer.

[4] S. A. Alimuddin, I. F. Ismail, A. N. Mohammed, and B. Basuno, "The Influence of Limiters on Davis-Yee and Harten-Yee TVD Schemes," *CFD Letters*, vol. 14, no. 9, pp. 15-31, 2022.

[5] S. Kaewta, N. Khansai, S. Sirisubtawee, and S. Phongthanapanich, "A comparison of TVD limiter functions for a convection–diffusion–reaction equation and Euler equations on triangular grids," *Journal of the Brazilian Society of Mechanical Sciences and Engineering*, vol. 44, no. 11, p. 500, 2022.

[6] L. Bessone, P. Gamazo, M. Dentz, M. Storti, and J. Ramos, "GPU implementation of Explicit and Implicit Eulerian methods with TVD schemes for solving 2D solute transport in heterogeneous flows," *Computational Geosciences*, vol. 26, no. 3, pp. 517-543, 2022.

[7] L. Krivodonova and A. Smirnov, "On the TVD property of second order methods for 2D scalar conservation laws," *arXiv preprint arXiv:2110.00067*, 2021.

[8] I. Ali, N. A. Malik, and R. Mehmood, "Finite Volume TVD Scheme for a Nonlinear Gas Transport Model in Shale Rocks," in *2019 8th International Conference on Modeling Simulation and Applied Optimization (ICMSAO)*, 2019, pp. 1-5: IEEE.

[9] A. Tasri, "Comparison of Errors Caused by Flux Limiters on the Numerical Solution of Advection-Diffusion Problem," *Nigerian Journal of Technological Development*, vol. 19, no. 4, pp. 309-315, 2022.

[10] M. Yadegari and M. Jahdi, "Capturing of Shock Wave of Supersonic Flow over the Bump Channel with TVD, ACM and Jameson Methods," *Iranian*

Journal of Mechanical Engineering Transactions of the ISME, vol. 22, no. 1, pp. 108-126, 2021.

[11] R. Lochab and V. Kumar, "High resolution TVD scheme based on fuzzy modifiers for shallow-water equations," in *Computational Science–ICCS 2021: 21st International Conference, Krakow, Poland, June 16–18, 2021, Proceedings, Part I*, 2021, pp. 480-492: Springer.

[12] S. Tang and M. Li, "Construction and application of several new symmetrical flux limiters for hyperbolic conservation law," *Computers & Fluids*, vol. 213, p. 104741, 2020.

[13] I. F. Ismail, B. Basuno, A. N. Mohammed, F. Ismail, and N. F. Mohd Yusof, "The Development of Euler Solver Based on Flux Vector Splitting and Modified TVD Schemes," in *Technological Advancement in Instrumentation & Human Engineering: Selected papers from ICMER 2021*: Springer, 2022, pp. 687-702.

[14] Ü. Osman, "Numerical Simulation of Convection-Diffusion Equation Using a Novel Flux Limiter," *Inspiring Technologies and Innovations*, vol. 1, no. 1, pp. 1-8.